Electronic and magnetic properties of single-crystal YNi_2B_2C from ^{11}B and ^{89}Y NMR and magnetic-susceptibility measurements

B. J. Suh,* F. Borsa,† D. R. Torgeson,‡ B. K. Cho,§ P. C. Canfield, D. C. Johnston, J. Y. Rhee,** and B. N. Harmon
Ames Laboratory and Department of Physics and Astronomy, Iowa State University, Ames, Iowa 50011
(Received 20 May 1996)

The quaternary intermetallic compound superconductor YNi_2B_2C with transition temperature $T_c=15.5$ K has been investigated by ^{11}B and ^{89}Y nuclear magnetic resonance (NMR) and by magnetic susceptibility χ measurements both in the normal and the superconducting states. The NMR and relaxation measurements have been performed in a powder sample and single crystals. ^{11}B ($I=3/2$) NMR spectra display patterns typical for an axially symmetric field gradient with quadrupole coupling frequency $\nu_Q=698\pm1$ kHz and ^{89}Y ($I=1/2$) data show spectra typical for a large anisotropic Knight shift, K, with axial symmetry ($3K_{ax}=0.042\%$). In the normal state, the ^{11}B K increases with decreasing temperature while ^{89}Y K decreases. The temperature dependences of both the isotropic (K_{iso}) and anisotropic ($3K_{ax}$) components of the ^{11}B and ^{89}Y Knight shifts are presented together with dc magnetic susceptibility (χ) measurements obtained from magnetization measurements and are explained by the sharp features of the density of states near the Fermi level in the system. The analysis of the NMR and $\chi(T)$ data when combined with the theoretical calculation of the Van Vleck contribution to $\chi(T)$ allows the determination of the hyperfine coupling constants for both nuclei investigated and permits the separation of the different contributions to the total measured $\chi(T)$. The nuclear spin-lattice relaxation rate (NSLR) (T_1^{-1}) results for ^{11}B show an enhancement of $(T_1T)^{-1}$ when lowering the temperature, consistent with previous results. It is shown that the enhancement of the ^{11}B NSLR is not due to the effects of antiferromagnetic fluctuations of Ni magnetic moments but simply due to the increase of the s-band spin susceptibility with decreasing temperature as reflected in the temperature dependence of the Knight shift. Contrary to the case of ^{11}B, the ^{89}Y NSLR displays a $(T_1T)^{-1}$ which is independent of temperature, indicating that the dominant contribution is from a large temperature-independent orbital Knight shift. In the superconducting state, the ^{11}B NSLR drops rapidly without a coherence peak and is found to fit BCS behavior with a superconducting gap parameter at $T=0$ given by $2\Delta_0=(3.4\pm0.5)k_BT_c$. [S0163-1829(96)01745-6]

I. INTRODUCTION

The recently discovered quaternary intermetallic compound superconductors, RNi_2B_2C (R=Sc, Y, Th or a rare-earth element),[1–5] have aroused great interest due to high superconducting transition temperatures, T_c (e.g., $T_c=16.6$ K for R=Lu) compared with most other intermetallic compounds, and due to the presence in the lattice of nickel, which in its elemental form is an itinerant ferromagnet. Furthermore the compounds containing the magnetic rare-earth ions R=Dy,[5] Ho, Er, and Tm (Ref. 2) also exhibit superconductivity. The structure[6] consists of a square lattice of Ni atoms bounded by B layers. These Ni_2B_2 layer blocks are separated and bonded together by YC layers. Thus the structure is qualitatively similar to those of the layered cuprate high-temperature superconductors (HTSC's). However, electronic band-structure calculations[7–12] indicate that these compounds are three-dimensional d-band metals and that superconductivity arises from the conventional electron-phonon mechanism. Compared to other intermetallic compounds, the relatively high T_c is thought to arise from a relatively high density of states at the Fermi energy.[9] Indeed, low-temperature heat-capacity measurements of YNi_2B_2C (Refs. 13–15) and $LuNi_2B_2C$ (Refs. 15 and 16) showed a relatively large electronic linear heat capacity coefficient $\gamma\approx19$ mJ/mol K^2.

An important issue is the magnetic behavior of the Ni layers because of their analogy with the Cu layers in HTSC. Preliminary NMR investigations have suggested the possibility of antiferromagnetic (AF) fluctuations of the Ni magnetic moments in YNi_2B_2C and $LuNi_2B_2C$ (Refs. 17–20) based on the deviation of the T dependence of the ^{11}B nuclear spin-lattice relaxation rate (NSLR) (T_1^{-1}) from the predictions of the Korringa relation $1/T_1T\propto K^2$. Our subsequent accurate measurements in a single crystal, briefly summarized in Ref. 21, have shown that when the temperature dependence of the Knight shift K is properly taken into account the ^{11}B NSLR obeys the Korringa relation without need to invoke the presence of AF correlations. In this paper we present the complete detailed investigation of both the ^{11}B and the ^{89}Y NMR and relaxation in single crystals of YNi_2B_2C. Measurements of magnetization, i.e., of dc magnetic susceptibility χ were also performed on the same single crystals. The analysis of the data is aided by the results of theoretical calculations of the bare spin and the Van Vleck contributions to the magnetic susceptibility. By combining the NMR data, the χ data and the theoretical estimates we separated the different contributions to the total measured $\chi(T)$ and established the temperature dependence and the anisotropy of each term. The analysis provides useful information on the hyperfine interactions and on the electronic properties of the system in its normal metallic state and gives strong evidence against the presence of AF correlations within the Ni sublattice. Finally, we report an estimate of the superconducting gap parameter Δ_0 at $T=0$ obtained from ^{11}B NSLR data below T_c,

which is found to be consistent with the BCS prediction for an *s*-wave superconductor.

II. EXPERIMENTAL DETAILS

Single crystals of YNi_2B_2C with $T_c=15.5$ K were prepared at Ames Laboratory by the method described in detail elsewhere.[22] ^{11}B and ^{89}Y NMR measurements were performed in a powder sample and in a stack of single-crystal plates of YNi_2B_2C having an approximate total volume of $10\times4\times1$ mm^3. The typical size of a single plate in the stack was approximately $3.5\times3.5\times0.3$ mm^3. The measurements were performed both in the normal and in the superconducting state with a pulse Fourier transform (FT) spectrometer in external fields H of 0.9, 1.2, 2.4, and 8.2 T. In particular, an accurate investigation of the normal state was made on the single crystals in an Oxford Instruments superconducting magnet at $H=8.2$ T with field inhomogeneity less than 0.1 G operating at 112 and 17.1 MHz for ^{11}B and ^{89}Y, respectively. The ^{11}B ($I=3/2$) NMR shifts of the central line were measured with respect to the resonance frequency in H_3BO_3 aqueous solution and for two orientations of magnetic field, $\mathbf{H}\|\mathbf{c}$ and $\mathbf{H}\perp\mathbf{c}$ (the c axis is perpendicular to the Ni layers). The ^{11}B NSLR's were measured using a single-pulse saturation method. The ^{89}Y ($I=1/2$) Knight shifts measurements were performed on the single crystals with the respect to YCl_3 aqueous solution for $\mathbf{H}\|\mathbf{c}$ and $\mathbf{H}\perp\mathbf{c}$. On the other hand, the ^{89}Y NSLR could be measured only on the powder sample with irradiation at the resonance frequency of the singularity corresponding to the resonance for the orientation $\mathbf{H}\perp\mathbf{c}$. This limitation is dictated by the poor signal-to-noise ratio in the stacked single crystals due to the limited penetration of the radio frequency into the bulk of the sample and the small filling factor of the single-crystal plates.

The dc magnetic susceptibility measurements were obtained from the ratio of the magnetization to the applied field. Magnetization measurements on a single crystal were carried out using a Quantum Design SQUID magnetometer for two field orientations in the normal state. A nonvanishing magnetization $M_0(T)\approx(0.15\pm0.05)$ G cm^3/mol at $H=0$ was obtained from the extrapolation of the linear $M(H)$ data for $1\leqslant H\leqslant5$ T to $H=0$ at each temperature. This effect was attributed to the presence of ferromagnetic impurities, equivalent to a concentration of ≈6 at ppm of iron metal with respect to Ni. The data in Fig. 4 below are corrected for this spurious contribution.

III. EXPERIMENTAL RESULTS

A. ^{11}B and ^{89}Y NMR spectra

The ^{11}B NMR spectrum is shown in Fig. 1 at room temperature measured both in a powder sample at 15 K [Fig. 1(a)] and single crystals at 300 K [Fig. 1(b)]. As shown in Fig. 1(b) both the central line ($+1/2\leftrightarrow-1/2$ transition) and the satellite transitions ($+3/2\leftrightarrow+1/2$ and $-3/2\leftrightarrow-1/2$ transitions) are relatively narrow (about 6 kHz) for both orientations of the magnetic field, $\mathbf{H}\|\mathbf{c}$ and $\mathbf{H}\perp\mathbf{c}$. This circumstance indicates that the single crystals are free of structural defects and that the alignment of the different crystals stacked with a common c axis is very good.

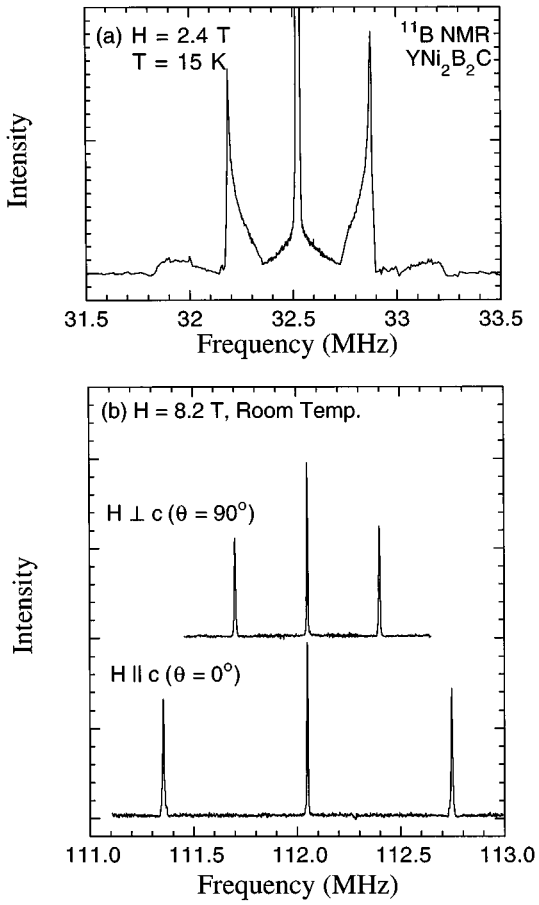

FIG. 1. ^{11}B NMR spectra in YNi_2B_2C: (a) in a powder sample and (b) in stacked single crystals.

The separation of the satellite transitions in first order perturbation theory obeys the simple relation[23]

$$\delta\nu=\frac{\nu_Q}{2}(3\cos^2\theta-1), \tag{1}$$

where the quadrupole coupling frequency is defined as $\nu_Q\equiv e^2qQ/2h$ in terms of the nuclear quadrupole moment Q and of the largest component q of the axially symmetric electric-field gradient. From the spectrum in Fig. 1(b) one derives $\nu_Q=(698\pm1)$ kHz at room temperature. No measurable change of the quadrupole interaction could be observed from 300 down to 15 K, indicating the absence of structural changes in this temperature range. It is noted that for $\mathbf{H}\|\mathbf{c}$ the position of the central line is not affected by quadrupole interactions while for $\mathbf{H}\perp\mathbf{c}$ the position of the central line is shifted by second-order quadrupole effects as $\nu_\perp=\nu_0+3\nu_Q{}^2/16\nu_L$, where ν_0 is the resonance frequency in the absence of the quadrupolar interaction and ν_L is the Larmor frequency.[23] Thus in order to measure the Knight shift at $H=8.2$ T ($\nu_L=112$ MHz) for the perpendicular orientation we subtracted 815 Hz from the observed resonance frequency.

The full width at half maximum of the central line is plotted in Fig. 2 as a function of temperature for two field orientations. At room temperature the NMR is inhomogeneously broadened as indicated by the presence of a spin echo following a $\pi/2$-π pulse sequence. The temperature de-

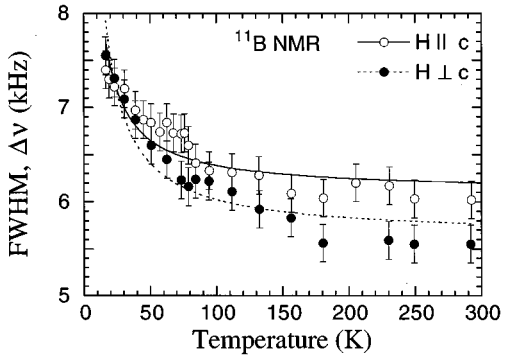

FIG. 2. ^{11}B NMR linewidth $\Delta\nu$ of the central lines vs temperature for two magnetic field orientations with respect to the crystal c axis: $\mathbf{H}\|\mathbf{c}$ and $\mathbf{H}\perp\mathbf{c}$ for $H=8.2$ T. The curves are fits $\Delta\nu=\Delta\nu_0+b\chi^{\rm imp}$ (see the text for details).

pendence, which becomes pronounced below 100 K, is a clear indication of a broadening mechanism associated with a random distribution of localized magnetic moments. The effect will be discussed further on in connection with the susceptibility measurements.

The ^{89}Y NMR spectrum at room temperature is shown in Fig. 3. The upper trace represents the powder pattern in a polycrystalline sample with the singularity corresponding to crystallites oriented with $\mathbf{H}\perp\mathbf{c}$ and the step corresponding to $\mathbf{H}\|\mathbf{c}$. The lower trace represents the NMR spectra in the single crystal for the two orientations of the magnetic field with respect to the c axis. The excellent correspondence on the frequency scale of the single-crystal signal and of the singularities in the powder pattern is worth noting.

B. Magnetic susceptibility measurements

The experimental data for the magnetic susceptibility χ as a function of temperature and orientation are shown in Fig. 4(a) where the data are corrected for the tentative contribution of small amounts of ferromagnetic impurities as discussed above. The main features are the quite large anisotropy of χ, $\chi_\perp-\chi_\|$ $(\equiv-3\chi_{\rm ax})$, and the considerable temperature dependence of both the isotropic component $\chi_{\rm iso}\equiv(\chi_\|+2\chi_\perp)/3$ and the anisotropic component, $-3\chi_{\rm ax}\equiv\chi_\perp-\chi_\|$. A weak Curie-type increase at low temperature ($<$50 K) is observed for $\chi_{\rm iso}$ but not for $\chi_{\rm ax}$. This effect is attributed to the presence of a small concentration of randomly distributed local magnetic moments which could be paramagnetic impurities. The separation of the different terms contributing to the measured susceptibility χ will be described in Sec. IV A.

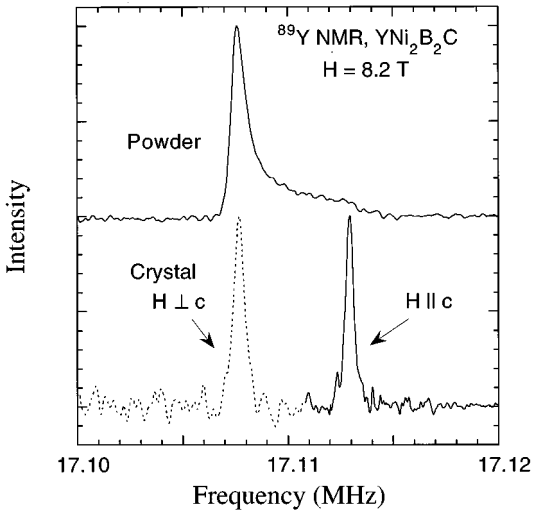

FIG. 3. ^{89}Y NMR spectra in YNi_2B_2C for $H=8.2$ T at 300 K. The upper trace is the spectrum in a powder and the lower traces are the spectra in stacked single crystals for two field orientations with respect to the c axis.

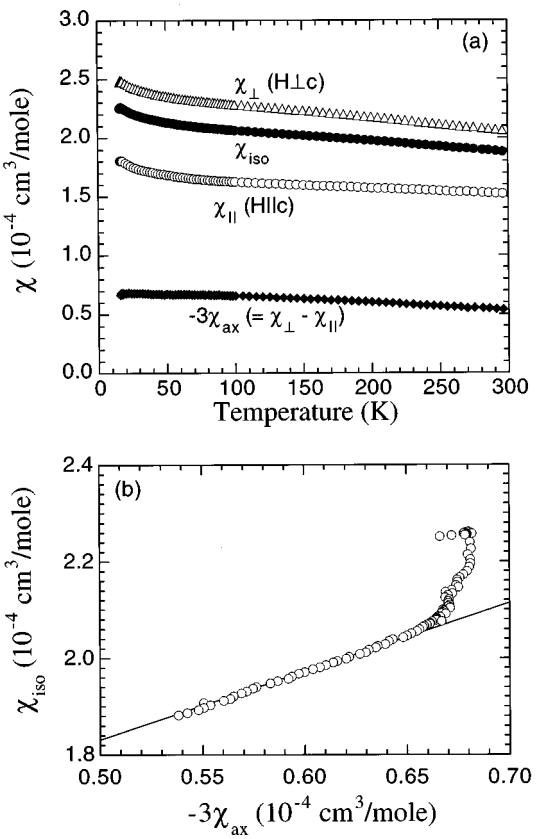

FIG. 4. (a) Magnetic susceptibility χ vs temperature in a YNi_2B_2C single crystal for two magnetic field orientations. (b) The isotropic component ($\chi_{\rm iso}$) vs the anisotropic component ($-3\chi_{\rm ax}\equiv\chi_\perp-\chi_\|$) of the susceptibility.

C. ^{89}Y Knight shift and nuclear spin-lattice relaxation rate

The temperature dependences of the ^{89}Y Knight shifts, ^{89}K, in stacked single crystals and in a powder sample are shown in Fig. 5 for $\mathbf{H}\|\mathbf{c}$ and $\mathbf{H}\perp\mathbf{c}$. For the powder sample the data refer to the singularity in the spectrum and thus represent the Knight shift of the crystallites with the c axis perpendicular to the field direction. The data in Fig. 5 are not corrected for the demagnetization effects and this is the reason why the $K_\perp$ data for the stacked single crystals are different from the corresponding $K_\perp$ data from the powder singularity. The data can be corrected for demagnetization effects by utilizing the relation[23]

$$K^m(T)\equiv\frac{\nu_m-\nu_L}{\nu_L}=K(T)+4\pi\left(\frac{1}{3}-D\right)\chi, \qquad (2)$$

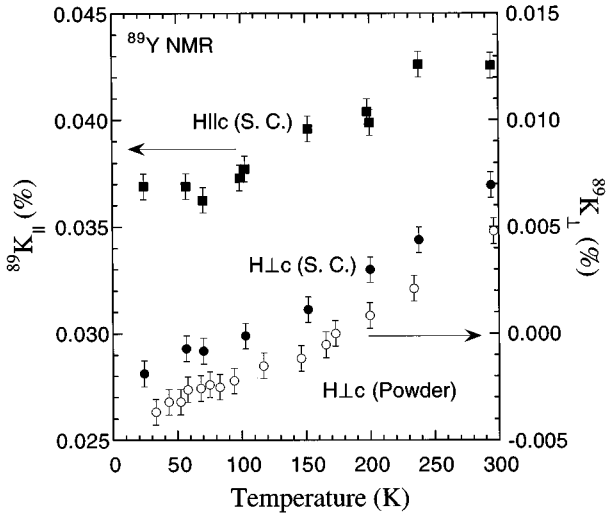

FIG. 5. ^{89}Y Knight shift ^{89}K vs temperature in YNi_2B_2C. The solid symbols denote (■) $^{89}K_{\parallel}$ ($\mathbf{H}\parallel\mathbf{c}$) and (●) $^{89}K_{\perp}$ ($\mathbf{H}\perp\mathbf{c}$), respectively, in stacked single crystals. Open circles (○) denote the shift of the resonance frequency of the singularity in the spectrum of the powder sample (see Fig. 3). The singularity is from the powder grains whose crystal orientation satisfies the condition, $\mathbf{H}\perp\mathbf{c}$.

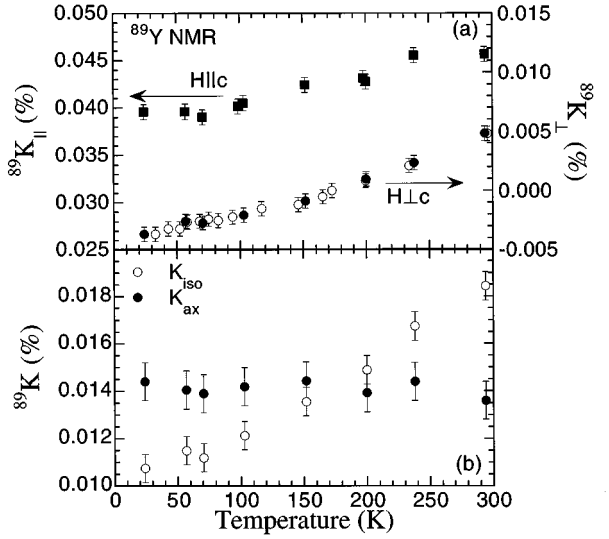

FIG. 6. (a) ^{89}Y Knight shift ^{89}K vs temperature and (b) the shift components $K_{\rm iso}$ and $K^{\rm ax}$ in YNi_2B_2C. The data are corrected for the demagnetization effects (see the text).

where D is the demagnetization factor and χ is the measured magnetic susceptibility. $K^m(T)$ is the measured shift shown in Fig. 5 while $K(T)$ is the correct Knight shift value. The χ in Eq. (2) is in dimensionless volume units and is obtained from the molar susceptibility data in Fig. 4 by multiplying by d/M with $M=239.9$ g/mol being the molar mass and $d=6.09$ g/cm^3, the mass density of YNi_2B_2C.

By using the measured values of volume susceptibility χ and assuming $D_\perp=1/3$ for a powder sample, we find that the average value of the demagnetization factor needed to match the $K_\perp$ data vs temperature in single crystals and in the powder sample is $D_\perp=0.06\pm0.02$. This value is in good agreement with the theoretical value,[24] $D_\perp=0.054$, estimated for the average dimensions $3.5\times3.5\times0.3$ mm^3 of the single-crystal plates. Assuming $D_a=D_b=D_\perp$ and using the relation $D_a+D_b+D_c=1$, we find $D_\parallel=D_c=0.88$. Here the factors of 0.88 and 0.06 take into account the deviations from the ideal thin slab geometry of our crystals. The Knight shifts, corrected according to Eq. (2) using the experimental $\chi(T)$ values in Fig. 4(a), are shown in Fig. 6(a). The quantities plotted in Fig. 6(b) are the isotropic ($K_{\rm iso}$) and anisotropic ($K_{\rm ax}$) components of the Knight shift tensor defined in the usual way: $K_{\rm iso}\equiv1/3(K_\parallel+2K_\perp)$ and $3K_{\rm ax}\equiv K_\parallel-K_\perp$.[23] The $K_{\rm ax}$ is seen to be temperature independent while $K_{\rm iso}$ decreases with decreasing temperature.

The ^{89}Y NSLR results are shown in Fig. 7 in a plot of $1/T_1T$ vs temperature. Since the measurements had to be performed in the powder sample no firm information about the anisotropy of the relaxation is available. The data in Fig. 7 were collected by irradiating at the frequency of the singularity in the NMR powder spectrum of Fig. 3 and thus refer mainly to the condition $\mathbf{H}\perp\mathbf{c}$. However, since the spectral width of the radio-frequency pulse also partly covers nuclei in crystallites with different orientations one would expect to see some nonexponentiality in the recovery of the nuclear magnetization if the NSLR's were strongly anisotropic. Since the recovery was found to be exponential one can deduce that the anisotropy of the NSLR, if present at all, is small relative to the isotropic component.

D. ^{11}B Knight shift and nuclear spin-lattice relaxation rate

The ^{11}B Knight shift (^{11}K) results are shown as a function of temperature and orientation of the external magnetic field in Figs. 8(a)–8(c) where the corrections for the second-order quadrupole effects and demagnetization effects have been done in the same ways as described above for the ^{89}Y Knight shift. Contrary to the results for ^{89}Y shown in Fig. 6, the anisotropic part of the ^{11}B Knight shift is more than 1 order of magnitude smaller than the isotropic part and both display a sizable temperature dependence. In addition, contrary to the relation between $\chi_{\rm iso}$ and $-3\chi_{\rm ax}$ in Fig. 4(b), one finds a good linear relation between $^{11}K_{\rm iso}$ and $^{11}K_{\rm ax}$ in the whole temperature range investigated as shown in Fig. 8(c).

The ^{11}B NSLR's are shown in Fig. 9 as a function of temperature and for the two orientations of the external magnetic field with respect to the c axis. The remarkable feature is that no measurable anisotropy of the NSLR is present, in

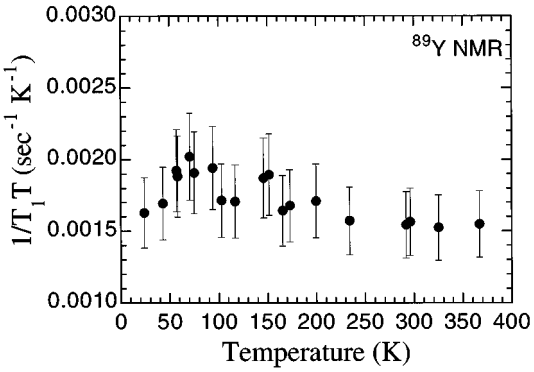

FIG. 7. Temperature dependence of ^{89}Y $(T_1T)^{-1}$ in a YNi_2B_2C powder sample.

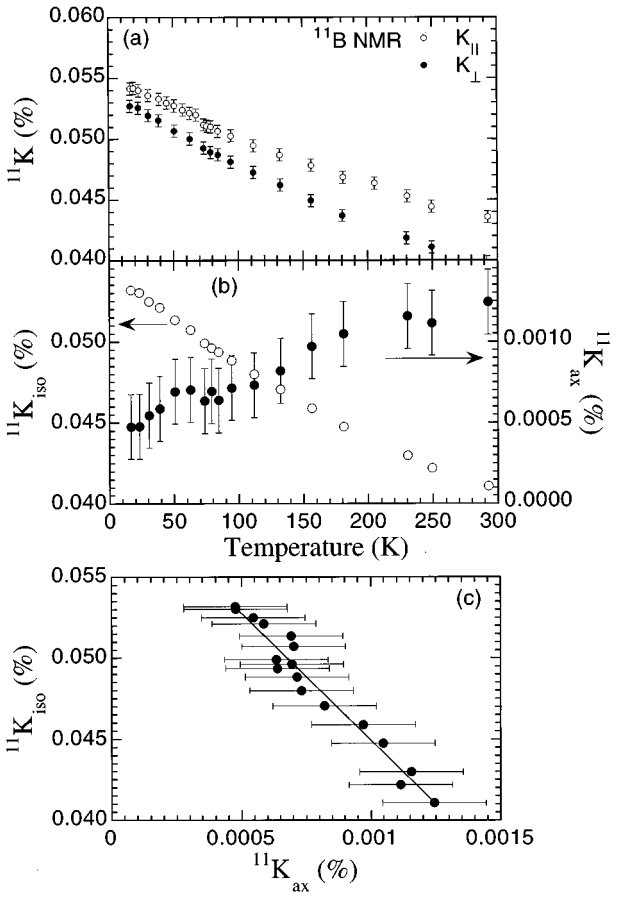

FIG. 8. ^{11}B Knight shift components of the central line in stacked YNi_2B_2C single crystals: (a) $^{11}K_{\|}$ ($\mathbf{H}\|\mathbf{c}$) and $^{11}K_{\perp}$ ($\mathbf{H}\perp\mathbf{c}$) vs temperature T, (b) $^{11}K_{iso}$ and $^{11}K_{ax}$ vs T, and (c) $^{11}K_{iso}$ vs $^{11}K_{ax}$. The data are corrected for the second-order quadrupolar and demagnetization effects.

contrast with both the susceptibility and the Knight shift results shown in Figs. 4 and 8, respectively.

IV. DISCUSSION

A. Separation of the magnetic susceptibility into its different contributions from calculations and experiments

The measured susceptibility χ can be partitioned as

$$\chi=\chi^{\rm imp}+\chi^{\rm sp}+\chi^{\rm orbit}$$
$$=\chi^{\rm imp}+\chi^{\rm sp}+\chi^{\rm Landau}+\chi^{\rm core}+\chi^{\rm VV}, \qquad (3)$$

where $\chi^{\rm imp}$ is an extrinsic defect or impurity contribution, $\chi^{\rm VV}$ is the Van Vleck orbital contribution, $\chi^{\rm Landau}$ is the orbital contribution due to conduction electrons, and $\chi^{\rm sp}$ is the Pauli spin susceptibility which can be temperature dependent in the presence of sharp features in the density of states (DOS) near the Fermi level.[23]

First we argue that χ must include a small contribution $\chi^{\rm imp}$ from randomly distributed localized magnetic moments. These moments could arise either from paramagnetic impurities in the sample or from a small percentage of localized Ni moments in the proximity of defects. The conclusion is based on the increase of the ^{11}B inhomogeneous linewidth

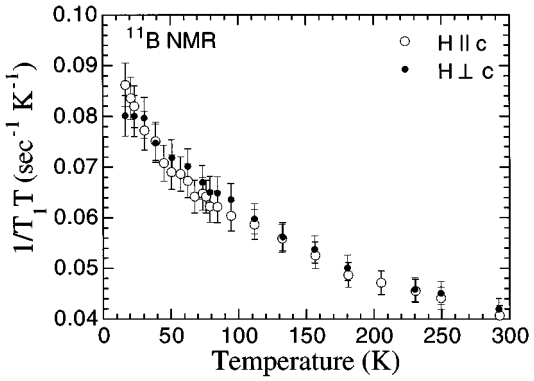

FIG. 9. Temperature dependence of ^{11}B $(T_1T)^{-1}$ in stacked YNi_2B_2C single crystals for $H=8.2$ T for both magnetic field orientations.

below 100 K (see Fig. 2) and the corresponding upturn of χ shown in Fig. 4. As further evidence, the Knight shifts shown in Fig. 8 do not track the linewidths and the susceptibilities below 100 K as expected; a random distribution of paramagnetic moments would broaden the line without affecting the shift of the center of the line, as observed.

In order to determine $\chi^{\rm imp}$ we first note that $\chi^{\rm imp}$ is isotropic, since $\chi_{\rm iso}(T)$ in Fig. 4(a) shows a Curie-like upturn below $\approx$50 K whereas $\chi_{\rm ax}(T)$ does not. Above 100 K we find that $\chi_{\rm iso}=P(-3\chi_{\rm ax})+Q$, where $P=1.09\pm0.02$ and $Q=(1.47\pm0.03)\times10^{-4}$ cm^3/mol, as shown in Fig. 4(b). We now assume that the intrinsic susceptibility $\chi^{\rm intr}_{\rm iso}$ below 50 K, where $\chi^{\rm imp}$ begins to contribute, is given by the same expression, $\chi^{\rm intr}_{\rm iso}(T)=P[-3\chi_{\rm ax}(T)]+Q$. Then, $\chi^{\rm imp}$ below 50 K is found: $\chi^{\rm imp}=\chi_{\rm iso}-\chi^{\rm intr}_{\rm iso}$. The obtained $(\chi^{\rm imp})^{-1}(T)$ is plotted in Fig. 10. The $\chi^{\rm imp}(T)$ data in Fig. 10 are described by a Curie-Weiss law

$$\chi^{\rm imp}=\frac{3.1}{T(K)+0.5\ \ {\rm K}}\ (10^{-4}\ \ {\rm cm^3\,K/mol}). \qquad (4)$$

At 16 K, $\chi^{\rm imp}$ represents about 9% of $\chi_{\rm iso}$. The concentration of impurities which accounts for $\chi^{\rm imp}$ in Eq. (4) is 830 molar ppm of local moments with $S=1/2$ and $g=2$. However, for magnetic rare-earth impurities with large effective moments the concentration would be lower, e.g., 40 molar ppm of Gd ($S=7/2$, $g=2$) impurities.

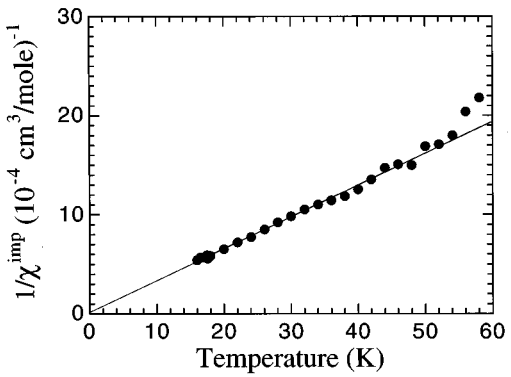

FIG. 10. Contribution of paramagnetic impurities to the susceptibility: $(\chi^{\rm imp})^{-1}$ vs temperature.

The broadening of the ^{11}B NMR line shown in Fig. 2 is consistent with the presence of the $\chi^{\rm imp}$ term in Eq. (4) due to randomly distributed paramagnetic moments. In this case one expects a contribution to the NMR linewidth proportional to $\chi^{\rm imp}$. The calculation of the NMR line shape and linewidth in the presence of comparable contributions from nuclear dipolar interactions and paramagnetic impurities is not trivial. However, one expects that the linewidth would contain a T-independent term $\Delta\nu_0$ due to the dipolar interaction plus a term proportional to the susceptibility of the impurities, i.e., $\Delta\nu(T)=\Delta\nu_0+b\chi^{\rm imp}(T)$.[25] In Fig. 2 we compare the experimental data with the curve for $\Delta\nu(T)$ obtained with $\Delta\nu_0=(6.1\pm0.3)$ kHz and $b=(0.9\pm0.07)\times10^{-5}$ kHz mol/cm^3 for $\mathbf{H}\|\mathbf{c}$ and $\Delta\nu_0=(5.6\pm0.4)$ kHz and $b=(1.3\pm0.1)\times10^{-5}$ kHz mol/cm^3 for $\mathbf{H}\perp\mathbf{c}$, respectively. Although the argument is only semiquantitative, the agreement found in Fig. 2 is sufficiently good to explain the observed NMR broadening.

We proceed now to estimate the other terms contributing to χ according to Eq. (3). Unfortunately, it is very difficult to obtain reliable estimates of $\chi^{\rm core}$ and $\chi^{\rm Landau}$ in intermetallic compounds such as YNi_2B_2C. Since $\chi^{\rm core}$ is proportional to the expectation value $\langle r^2\rangle$ of the square of the radius r for the core electrons,[23] this term is very sensitive to the radial distribution function of outer core electrons around the nucleus. In ionic compounds for which $\langle r^2\rangle$ is smallest, one typically uses standard tables such as Ref. 26 to estimate $\chi^{\rm core}$. For example, if YNi_2B_2C were considered to be an ionic compound (which it is not) containing the ions Y^{+3}, Ni^{+2}, B^{+3}, and C^{+4}, from Ref. 26 one would obtain $\chi^{\rm core}=-36.5\times10^{-6}$ cm^3/mol YNi_2B_2C. On the other hand, the contributions of the same atoms to $\chi^{\rm core}$ in intermetallic compounds, for which the respective $\langle r^2\rangle$ values are larger, are calculated[23] to be (in 10^{-6} cm^3/mol): -56.9 for Y, -29.5 for Ni, -12.6 for B, and -11.3 for C, yielding

$$\chi^{\rm core}=-1.52\times10^{-4}\ \text{cm}^3/\text{mol}\ \ YNi_2B_2C. \tag{5}$$

The magnitude of this value is more than a factor of 4 larger than the above magnitude for the ionic case, and illustrates the large differences in $\chi^{\rm core}$ that can arise in different compounds. In the absence of a band theory value of $\chi^{\rm core}$ for YNi_2B_2C, below we will utilize the value given in Eq. (5) with the caveat that the accuracy of this value is unclear.

The Landau contribution due to the orbital motion of the conduction electrons in the quasifree electron approximation for a spherical Fermi surface is given by $\chi^{\rm Landau}=(-1/3)(m/m^*)^2\chi^{\rm sp}_{\rm free}$, which is negative definite, where m is the electron mass, m^* is the band effective mass and $\chi^{\rm sp}_{\rm free}$ is the spin susceptibility of an equal concentration of free electrons. However, this expression is not necessarily applicable to transition metals, for which $\chi^{\rm Landau}$ can even be positive instead of negative.[27] We speculate that the magnitude of $\chi^{\rm Landau}$ is small compared to that of $\chi^{\rm core}$ and, given the uncertainty in the value of $\chi^{\rm core}$, we will assume that $\chi^{\rm Landau}=0$ in Eq. (3).

In order to obtain estimates of the bare density of states (DOS) at the Fermi energy E_F, $N(E_F)$, and of the Van Vleck contribution $\chi^{\rm VV}$, we first calculated the energy band structure using the scalar-relativistic, tight-binding, atomic-sphere-approximation, linear-muffin-tin orbital (ASA-LMTO) method. The exchange-correlation effects were included within the local-density approximation. In generating the self-consistent charge and potential, 641 irreducible **k** points were used. The muffin-tin radii used for the calculation were 3.628, 2.775, 1.714, and 1.715 a.u. for Y, Ni, B, and C, respectively. The resultant band structure was in good agreement with the result of Lee *et al.*[9] For the DOS calculation the whole reciprocal unit cell was divided into $40\times40\times40$ parallelepipeds, and energies and wave functions were calculated at 4531 irreducible **k** points. The bare DOS at E_F is found to be $N(E_F)=4.20$ states/eV f.u. (''f.u.'' means formula unit of YNi_2B_2C) which is comparable with previous values 4.09 states/eV f.u. for YNi_2B_2C (Ref. 9) and 4.8 states/eV f.u. for $LuNi_2B_2C$.[8] The angular-momentum- and site-decomposed DOS are summarized in Table I.

TABLE I. The angular-momentum- and site-decomposed DOS at the Fermi level. All are in units of eV^{-1} atom^{-1}.

Site	*s*	*p*	*d*
Y	0.018	0.040	0.679
Ni	0.044	0.236	1.197
B	0.030	0.135	
C	0.036	0.152	

The Van Vleck susceptibility is given by

$$\chi^{\rm VV}=\frac{2}{V}\mu_B^2\sum_{i,f,k}\frac{f_{\rm FD}(E_i)[1-f_{\rm FD}(E_f)]|\langle f|\mathbf{L}|i\rangle|^2}{E_f-E_i}, \tag{6}$$

where V is the unit cell volume, μ_B is the Bohr magneton, E_f and E_i are the energies of final (empty) and initial (occupied) states, respectively, and $f_{\rm FD}(E)$ is the Fermi-Dirac distribution function. We used the same linear tetrahedron method as in the DOS calculation for **k** space integration with 10 125 tetrahedra in 1/16 of the Brillouin zone. The detailed method of calculation is explained in Ref. 28. The calculated value of $\chi^{\rm VV}\equiv\chi^{\rm VV,cal}$ is 1.77×10^{-4} and 1.51×10^{-4} cm^3/mol at $T=0$ for $\mathbf{H}\|\mathbf{c}$ and $\mathbf{H}\perp\mathbf{c}$, respectively. We also calculated the temperature dependence of $\chi^{\rm VV}$ by employing a finite-temperature Fermi-Dirac distribution function when the **k** space integration was performed. It showed only a small temperature dependence, i.e., about a 2% decrease in magnitude from 0 to 300 K. The $\chi^{\rm VV,cal}(T)$ results are shown in Fig. 11.

Figure 11 also shows the different components of χ, after subtraction of $\chi^{\rm core}$. The $\chi^{\rm sp}(T)$ obtained from Eq. (3) by subtracting from χ the various contributions estimated as described above is anisotropic and temperature dependent. We now test $\chi^{\rm sp}(T)$ for consistency with band theory. Since we already have the total and angular-momentum- and site-decomposed DOS, the unenhanced spin susceptibilities can be calculated by[29]

$$\chi^{\rm sp.cal}(T)=\frac{\mu_B}{H}[n_+(T)-n_-(T)], \tag{7}$$

where μ_B is Bohr magneton and n_+ and n_- are, respectively, the numbers of electrons with spin up $(+)$ and spin down $(-)$ in an external field H, and $n_\pm(T)$ is given by

$$n_\pm(T)=\int N_\pm(E)f_{\rm FD}(E,T)dE, \tag{8}$$

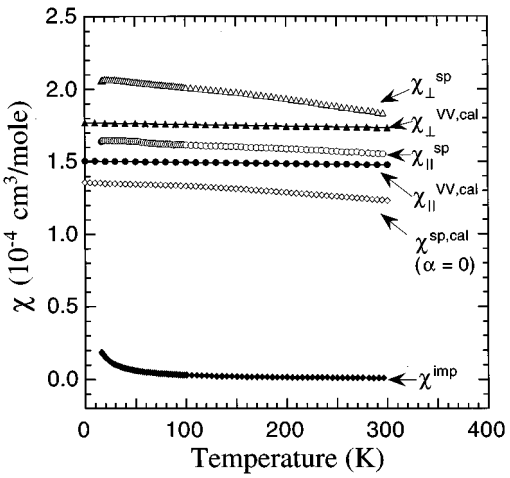

FIG. 11. Separation of the measured magnetic susceptibility of a YNi_2B_2C single crystal into the spin χ^{sp} and paramagnetic impurity χ^{imp} contributions vs temperature. The Van Vleck $\chi^{VV,calc}$ and bare ($\alpha=0$) isotropic spin $\chi^{sp,calc}$ susceptibilities calculated from the band structure are also shown.

where $N_{\pm}(E)=\frac{1}{2}N(E\pm\Delta E)$. To determine $N_{\pm}(E)$ we divide the total DOS into two halves and shift them by $\Delta E=\mu_B H$ in energy. We used $H=8.2$ T as in the NMR experiment, and have assumed a Landé factor $g=2$. In the calculation of $n_{\pm}(T)$ the temperature-dependent chemical potential is determined by making $n_+ + n_- = n$, where $n=33$ is the total number of electrons in an unit cell. The calculated $\chi^{sp,cal}(T=0)$ is 1.36×10^{-4} cm^3/mol. The complete temperature dependence is plotted as $\chi^{sp,cal}(T)$ in Fig. 11, where the predicted $\chi^{sp,cal}$ is seen to decrease with T, about 10% from $T=0$ to 300 K, as observed in the $\chi^{sp}(T)$ derived from the data. In the same way only the boron s-electron contribution ($\chi^{sp}_{B,s}$) to χ^{sp} and its temperature dependence were also calculated, yielding about a 6% decrease from $T=0$ to 300 K. The average χ^{sp} extrapolated at $T=0$ is $\chi^{sp}_{iso}\equiv(\chi^{sp}_{\parallel}+2\chi^{sp}_{\perp})/3=1.93\times10^{-4}$ cm^3/mol. The ratio of experimental to bare band values is $F=1.4$, which should be the same as the Stoner exchange enhancement factor $(1-\alpha)^{-1}$ of χ^{sp}. Our value $F=1.4$ is indeed comparable with the values of $(1-\alpha)^{-1}$ calculated from band theory for YNi_2B_2O [1.82 (Ref. 9)] and $LuNi_2B_2C$ [1.3±0.2 (Ref. 8)]. Given the uncertainty in χ^{core} and χ^{Landau} discussed above, this agreement is to some extent fortuitous. The anisotropy in χ^{sp} in Fig. 4 presumably arises for anisotropy in the g factor, for which band calculations are not available.

B. Knight shift and magnetic susceptibility

1. ^{11}B NMR

Since there are no d electrons at the boron site as seen in Table I and the hyperfine coupling constant for core polarization or exchange interaction is relatively small compared with the contact hyperfine coupling constant one may neglect any contribution to $^{11}K_{iso}$ from core polarization or exchange interaction and orbital terms related to χ^{VV}.[23] Thus the ^{11}B Knight shift can be written as

$$^{11}K_{iso}(T)=\,^{11}A_s^{at}\xi\chi^{sp}_{B,s}(T), \tag{9}$$

where $\chi^{sp}_{B,s}(T)$ is the spin susceptibility contribution of the boron $2s$-band electrons at the Fermi surface and $^{11}A_s^{at}$ is the atomic boron contact hyperfine interaction:[23]

$$^{11}A_s^{at}=1\times10^6 G/N_A\mu_B=179\ \text{mol B/cm}^3. \tag{10}$$

The factor $\xi=\langle|\psi(0)|^2\rangle_F/|\psi(0)|^2$ takes into account the difference between the probability density at the nucleus of the $2s$ wave function for electrons in the metal and in the atom. The factor ξ is slightly greater than one in normal metals due to the normalization of the wave function over a Wigner-Seitz cell, which has a smaller volume than the volume over which the atomic wave function extends.[23] Note that in Ref. 23 the Knight shift is expressed in terms of the total spin susceptibility. Thus if the spin susceptibility has contributions other than s terms the ξ factor derived from the measured Knight shift can be considerably less than one.[23] In Eq. (9) we have expressed the Knight shift in terms of the s part of the susceptibility. Thus it is appropriate to assume $\xi\approx1$. Then from $^{11}K_{iso}(T)$ in Fig. 8(b), one derives $\chi^{sp}_{B,s}(20\ \text{K})=2.5\times10^{-6}$ cm^3/mol B. The ratio of this $\chi^{sp}_{B,s}$ to the total χ^{sp}_{iso} from Fig. 11 is $r=\chi^{sp}_{B,s}(20\ \text{K})/\chi^{sp}_{iso}(20\ \text{K})=0.013$ which compares well with the corresponding band-structure result $r=N_{B,s}(E_F)/N(E_F)=0.03/4.2$ (Table I)$=0.007$, where $N_{B,s}(E_F)$ is the s-electron density of states at E_F at the boron site. Thus the $^{11}K_{iso}$ probes only the local $N_{B,s}(E_F)$ at the B site and, in particular, not the d-band contribution of the Ni atoms to $N(E_F)$. The unusually large T dependence of $\chi^{sp}_{B,s}(T)$ which can be seen from Eq. (9) and the $K_{iso}(T)$ data in Fig. 8(b) is evidently a consequence of a strongly varying $N_s(E_F)$ near E_F. The $K_{iso}(T)$ for ^{11}B in YNi_2B_2C can be compared and contrasted with that in $LuRh_4B_4$.[30] In $LuRh_4B_4$ the ^{11}B Knight shift is independent of T in spite of the significant T dependence of χ, implying (i) no coupling of ^{11}B with d electrons, consistent with our Eq. (9) for YNi_2B_2C, and (ii) a T-independent $\chi^{sp}_{B,s}$, which contrasts with our T-dependent $\chi^{sp}_{B,s}$ inferred above for YNi_2B_2C. It is noted that the band theory calculation of $\chi^{sp}_{B,s}$ at the B site yields a reduction of only 6% from $T=0$ to room temperature while the $^{11}K_{iso}(T)$ data in Fig. 8 indicate a much larger effect ($\approx$20%). This discrepancy remains unexplained.

The anisotropic component of the Knight shift tensor is due to dipolar interaction of the $2p$ electrons with the ^{11}B nucleus. For the case of axial symmetry one has:[31]

$$K_{ax}(T)=\frac{1}{3}(K_{\parallel}-K_{\perp})=A_{ax}\chi^{sp}_p=\frac{1}{N_A}q_F\chi^{sp}_p(T)$$

with

$$q_F=\left\langle\int_{\text{atomic volume}}\psi^*_{k,n}(r)\left[\frac{3\cos^2\theta_k-1}{r^3}\right]\psi_{k,n}(r)d^3r\right\rangle_{FS}. \tag{11}$$

In this equation the dipolar interaction is averaged over the boron p electrons at the Fermi surface, θ_k being the angle between the tetragonal c axis and the vector joining the nucleus and the electron. The subscript n in the wave function is the index of a band whose energy eigenvalue is the same as the Fermi level. The local spin susceptibility of p electrons at the B site can be estimated by scaling the total susceptibility in Fig. 11, $\chi^{sp}_{iso}(20\ \text{K})=1.9\times10^{-4}$ cm^3/mol

YNi_2B_2C, by the ratio of the density of states from Table I, $N_{B,p}(E_F)/N(E_F)=0.135/4.2=3.2\times10^{-2}$, yielding $\chi^{sp}_{B,p}(20\ K)=6\times10^{-6}$ cm^3/mol B. Thus from $^{11}K_{ax}\cong0.0005\%$ in Fig. 8 and from Eq. (11) one estimates $q_F\cong5\times10^{23}$ cm^{-3}. The value of the hyperfine constant q_F was calculated by using the linear tetrahedron method in performing the **k**-space integration. In the linear tetrahedron method the Fermi surface is planar within a tetrahedron. Therefore the shape of the Fermi surface is either a triangle or a quadrangle. We assumed that the integration in Eq. (11) is uniform on the Fermi surface within a tetrahedron and we can write

$$q_F=\sum_i\left(\int_{\text{atomic volume}}\psi^*_{k,n}(r)\times\left[\frac{3\cos^2\theta_k-1}{r^3}\right]\psi_{k,n}(r)d^3r\right)\Delta S_{F,i}\Big/S_F, \quad (12)$$

where $\Delta S_{F,i}$ is the area of the Fermi surface at the ith tetrahedron and $S_F=\Sigma\Delta S_{F,i}$ is the total area of the Fermi surface in one unit cell of the reciprocal lattice. Since the 17th, 18th, and 19th bands cross the Fermi surface, we have three different sheets of Fermi surface and three q_F's. We add their contributions and obtain $q_F=8.01\times10^{23}$ cm^{-3} which is comparable with the experimental result $q_F\cong5\times10^{23}$ cm^{-3}.

2. ^{89}Y NMR

Since the density of d-electron states at the Y site is large (Table I) the ^{89}Y Knight shift has important contributions from both orbital terms and indirect and/or exchange polarization terms:

$$^{89}K_{iso}=^{89}K^{sp}+^{89}K^{orbit}=^{89}A\chi^{sp}_{iso}+B\chi^{VV}_{iso}, \quad (13a)$$

$$^{89}K_{ax}=N_A^{-1}q_F\chi^{sp}_{sp,d}+B\chi^{VV}_{ax}, \quad (13b)$$

where the first term in Eq. (13a) can contain both a positive contribution from the contact hyperfine interaction averaged over the s-wave function at the Fermi level and a negative contribution from core polarization and/or exchange polarization of s electrons at the Y site with polarized d-conduction electrons. In Eq. (13b) the first term is due to the dipolar interaction averaged over the p and d electrons at the Y site (we neglect here the anisotropy of the spin susceptibility) while the second term depends upon the anisotropy of the Van Vleck susceptibility.

We plot in Fig. 12 the measured $^{89}K_{iso}$ from Fig. 6(b) as a function of the isotropic spin susceptibility from Fig. 11 with the temperature as implicit parameter. Since χ^{VV} is almost T independent we can estimate from the fit in Fig. 12 the parameters in Eq. (13a) as $^{89}K^{orbit}_{iso}=0.095\pm0.01\%$ and $^{89}A=-4.4\pm0.8$ mol YNi_2B_2C/cm^3 with the large uncertainty due to the poor signal-to-noise ratio of the ^{89}Y NMR. The negative value found for the hyperfine constant ^{89}A implies that the dominant contact interaction is via indirect exchange polarization of Y s band and/or core electrons by the d electrons, a situation found also in the layered cuprate high-T_c superconductors.[32] In analogy to Eq. (9), we can write $^{89}K^{sp}=^{89}A\chi^{sp}_{iso}=^{89}A^{at}_d\xi\chi^{sp}_{Y,d}$ by neglecting the small s-electron contribution to the $^{89}K_{iso}$, where $\chi^{sp}_{Y,d}$is the spin susceptibility contribution of the yttrium $4d$-band electrons at the Fermi surface. Assuming $\xi\cong1$ and using the ratio $\chi^{sp}_{iso}/\chi^{sp}_{Y,d}\cong N(E_F)/N_{Y,d}(E_F)=4.2/0.679=6.2$ obtained from Table I we have $A^{at}_d=6.2\times{}^{89}A\cong-(27\pm5)$ mol Y/cm$^3\cong-(81\pm15)$ mol electron/cm^3 (for Y^{+3}) which is comparable with the value of core-polarization hyperfine interaction constant ≈-350 kG/$N_A\mu_B=-63$ mol electron/cm^3 for unpaired $4d$ valence electrons.[23] Since $^{89}K_{ax}$ in Fig. 6(b) is practically T independent one can argue that the anisotropic Knight shift is likely dominated by the second term in Eq. (13b) which has a negligible T dependence. However, the positive sign of $^{89}K_{ax}$ in Fig. 6(b) is opposite to the sign of χ^{VV}_{ax} in Eq. (13b) a circumstance which could be explained only by assuming that the orbital hyperfine constant B in Eq. (13b), is itself anisotropic with sign opposite to that of χ^{VV}_{ax}.

C. ^{11}B NSLR and absence of antiferromagnetic fluctuations

The same contact hyperfine interaction in Eq. (9) which is responsible for $^{11}K(T)$ is also responsible for the ^{11}B $T_1^{-1}(T)$, according to the Korringa relation $1/T_1T\propto K^2$.[23] To test this relation, T_1^{-1} vs K^2T/S is plotted in Fig. 13(a), where for the ^{11}B nucleus $S\equiv(\gamma_e/\gamma_n)^2h/8\pi^2k_B=2.55\times10^{-6}$ sec K, and $K(T)\equiv K_{iso}(T)$ based on the fact that the T_1^{-1} data for the two field orientations in Fig. 9 are the same within experimental error. The very good linear fit to the data in Fig. 13(a) indicates that the Korringa relation holds, but that there is a small contribution $(T_1^{-1})^{imp}$ to T_1^{-1} from the paramagnetic impurities detected in the above $\chi(T)$ (see Figs. 4 and 10) and in ^{11}B NMR linewidth (see Fig. 2) measurements. The $(T_1^{-1})=0.38$ sec^{-1} found here is of the same order of magnitude (after normalization for the different nuclear gyromagnetic ratios) as the contribution to the proton NSLR in metal hydrides containing ≈100 ppm of Gd impurities,[33] which in turn is comparable to the equivalent of 40 molar ppm of Gd impurities giving rise to the $\chi^{imp}(T)$ discussed above.

After subtracting $(T_1^{-1})^{imp}$ from the measured T_1^{-1}, the Korringa ratio $\kappa\equiv K^2T_1T/S$ is plotted in Fig. 13(b). One expects $\kappa=1$ for a Fermi gas,[23] whereas $\kappa\cong(1-\alpha)^{-1}$ in the presence of exchange enhancement of χ^{sp}.[34] From Fig. 13(b) we find a T-independent $\kappa=1.6\pm0.2$, in good agreement with the value $(1-\alpha)^{-1}=F=1.4$ obtained above from the analysis of $\chi(T)$ and from the above-cited band calculations.[8,9] We conclude that the decrease of $1/T_1T$ with

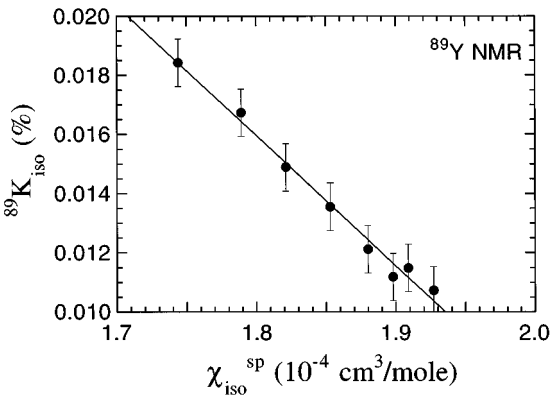

FIG. 12. ^{89}Y K_{iso} vs χ^{sp}_{iso} in YNi_2B_2C. The line is a linear fit using Eq. (4), yielding $^{89}A=-4.4\pm0.8$ mol YNi_2B_2C/cm^3 and $^{89}K^{orb}_{iso}=0.095\pm0.01\%$.

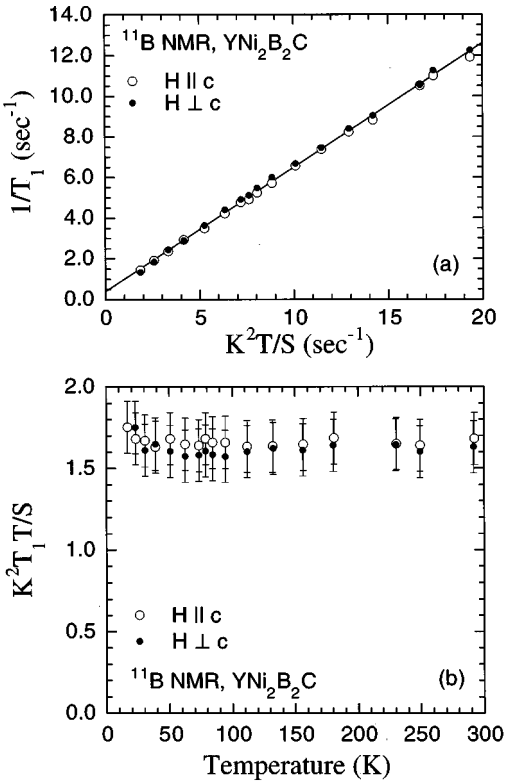

FIG. 13. (a) ^{11}B T_1^{-1} for $\mathbf{H}\|\mathbf{c}$ and $\mathbf{H}\perp\mathbf{c}$ vs K^2T/S. The line is the linear fit $1/T_1=0.38\ \mathrm{sec}^{-1}+0.61(K^2T/S)$ to all the T_1^{-1} data, where $K\equiv{}^{11}K_{\mathrm{iso}}$. (b) Korringa ratio $(K^2T_1T)/S$ vs temperature. The data are corrected for the paramagnetic impurity contribution $(1/T_1)^{\mathrm{imp}}=0.38\ \mathrm{sec}^{-1}$ from (a).

T in Fig. 9 and also observed in Refs. 17–20 for ^{11}B in YNi_2B_2C is simply a reflection of the decrease in $\chi^{\mathrm{sp}}_{B,s}$ and therefore in K_{iso} with T, which in turn arise from sharp features in $N_{B,s}(E)$ near E_F in YNi_2B_2C, a band-structure effect. Thus, one does not need to invoke AF correlations to explain the $(T_1T)^{-1}(T)$ data. From the above, we also infer that the nonlinearity in the $1/T_1T$ vs K^2 plot in Ref. 19 is due to paramagnetic impurities and not to antiferromagnetic (AF) correlations as suggested.

We concluded above that $(T_1T)^{-1}$ and $K(T)$ for the ^{11}B NMR are both driven by the same hyperfine interaction with the conduction s electrons at the B site and that these data are consistent with band theory. On the other hand, one could argue that since these measurements are only sampling the s electrons at the B site, they may not be sensitive to AF correlations among the d electrons associated with the Ni sublattice. Although this issue is difficult to address quantitatively in the absence of a specific model and parameters, we will examine one possible scenario. The ^{11}B nucleus in YNi_2B_2C occupies a site symmetry where AF correlations of local Ni moments coupled by the dipolar interaction to the ^{11}B nuclear would not be canceled, whereas indirect exchange coupling would cancel for commensurate AF correlations but not for incommensurate correlations. For the least favorable case of detecting commensurate correlations, the contribution to T_1^{-1} due to dipolar coupling, in the limit of high T where the Ni moments are uncorrelated, would be $(1/T_1)^{\mathrm{dip}}\approx 4\gamma_n^2\langle h^2\rangle/\omega_e$, where γ_n is the ^{11}B nuclear gyromagnetic ratio, $\langle h^2\rangle$ is the average square magnetic induction seen by a B nucleus due to a fluctuating Ni magnetic moment and $\omega_e=[(8/3)J^2nS(S+1)]^{1/2}/\hbar$ is the exchange frequency of the Ni moments with interatomic exchange coupling constant J and the number of nearest-neighbor magnetic ions n.[35] We estimate an upper limit $J/k_B\sim 100$ K from the T at which the rate of increase in χ^{sp} with decreasing T in Fig. 11 appears to decrease. Assuming a local Ni moment of $1\mu_B$, we find $(T_1^{-1})^{\mathrm{dip}}\approx 20\ \mathrm{sec}^{-1}$. This value is about a factor of 3 larger than the T_1^{-1} measured at 100 K in Fig. 9. With decreasing T, the $(T_1^{-1})^{\mathrm{dip}}$ contribution would be easily detectable as a decrease of κ in Fig. 13(b) on lowering T and by a strong depression of κ from the band theory value $(1-\alpha)^{-1}$, contrary to observation.

We note that $\chi^{\mathrm{imp}}(T)$ could not arise from a small magnetic moment localized at the Ni site, since in that case one would not expect an extra broadening of the line, contrary to our results as shown in Fig. 2. One would also expect a T-dependent ($\sim 1/T$) dipolar contribution to $^{11}K_{\mathrm{ax}}$ but not to $^{11}K_{\mathrm{iso}}$, due to the powder average of the local dipolar field at the B site, again contrary to our observation that $^{11}K_{\mathrm{ax}}$ scales linearly with $^{11}K_{\mathrm{ax}}$ over the entire T range 16–300 K of our measurements [Fig. 8(c)].

Therefore, from the consistency of both the χ and NMR data with band theory, we conclude that no antiferromagnetic correlations or local magnetic moments of nickel are present in YNi_2B_2C, as briefly discussed in our preliminary report.[21]

D. ^{89}Y NSLR

The ^{89}Y NSLR data in Fig. 7 show an almost constant behavior of $(T_1T)^{-1}$. Since the ^{89}Y Knight shift is the sum of an orbital and a spin contribution [see Eqs. (13a) and (13b)] it is reasonable to also expect two contributions to the NSLR:

$$S(T_1T)^{-1}=[K^d(T)]^2+R^{\mathrm{orb}}, \tag{14}$$

where $K^d(T)$ is the core polarization contribution to the Knight shift, which was written in Eq. (13a) as $^{89}A\chi_{\mathrm{iso}}(T)$, and R^{orb} is the orbital contribution to the NSLR which, however, is not proportional to the orbital Knight shift $K_{\mathrm{iso}}^{\mathrm{orb}}$ in Eq. (13a). The coefficient S is $S\equiv(\gamma_e/\gamma_n)^2(h/8\pi^2k_B)=1.09\times10^{-4}$ sec K for the ^{89}Y nucleus. Unfortunately there is no simple way to separate the two contributions to the NSLR in Eq. (14). Since from Fig. 7 it appears that $(T_1T)^{-1}$ is practically temperature independent while $K^d(T)$ in Eq. (14) has the temperature dependence of the spin susceptibility (Fig. 4), we tentatively conclude that the NSLR of ^{89}Y has a sizable contribution from the T-independent orbital term in Eq. (14). In any case there is no evidence for any contribution due to AF fluctuations of the Ni moments.

E. ^{11}B NSLR in the superconducting state

Figure 14 shows the ^{11}B NSLR in a powder sample at 1.2 and 2.4 T both in the normal and in the superconducting state. The ^{11}B NSLR in the normal state displays the enhancement with lowering temperature as discussed already and the enhancement is found to be field independent. In the superconducting state, a Hebel-Slichter (HS) coherence peak, which is expected to appear just below T_c for a conventional superconductor,[36] was not observed in the measurements at $H=1.2$ and 2.4 T (see Fig. 14). The results are very similar to those previously obtained by Hanson *et al.*[18] at $H=1.105$

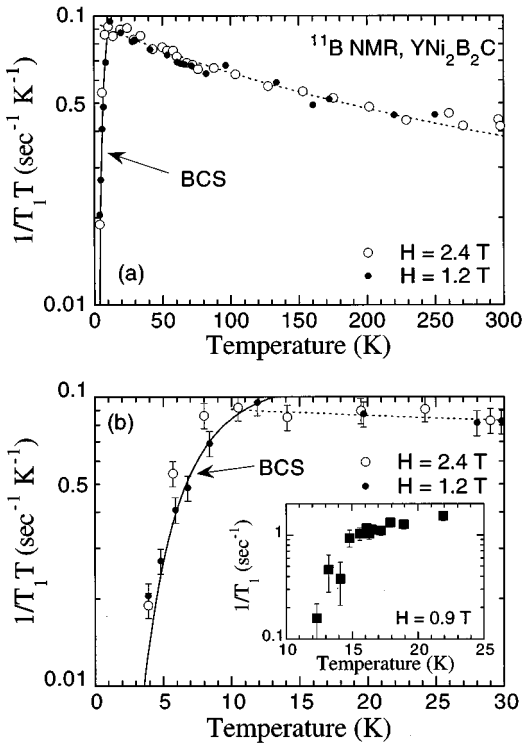

FIG. 14. $(T_1T)^{-1}$ of ^{11}B vs temperature in a YNi_2B_2C powder sample for two magnetic field intensities. The solid line is a fit of the data below T_c at $H=1.2$ T using BCS theory [see Eq. (15)] with $\Delta_0/k_B=18.6\pm0.7$ K. Note the different temperature scales in (a) and (b). The inset of (b) is the plot of T_1^{-1} vs temperature for $H=0.9$ T.

T and by Kohara *et al.*[20] at $H\approx1.4$ T. The HS peak can be reduced by the presence of impurities and/or by the applied magnetic field. In order to check these two possibilities we have performed measurements in a new powder sample obtained by grinding high-quality single crystals and at the lowest magnetic field ($H=0.9$ T) for which the ^{11}B NMR signal was still measurable in the superconducting state. As shown in the inset of Fig. 14(b), we observed a sharp drop of T_1^{-1} at T_c without any noticeable enhancement. We conclude that for the conditions of our experiments no HS peak is present. This could be due either to an applied field (0.9 T) which is still too large or to a reduction in the peak height arising from a small energy-gap anisotropy.[37]

The relaxation rate T_1^{-1} values at 1.2 T can be fit using the BCS theory given by[37]

$$\frac{1}{T_1}\propto\exp\left(-\frac{\Delta_0}{k_BT}\right), \tag{15}$$

with $\Delta_0/k_B=(18.6\pm0.7)$ K, where Δ_0 is the superconducting gap parameter, as shown by the solid curve in Fig. 14(b). A similar $\Delta_0=17(3)$ K was obtained from ^{11}B $1/T_1$ measurements.[18] The superconducting transition temperature T_c was measured from the initial detuning of the NMR tank circuit which is equivalent to measuring the change of the inductance of the system and the result is $T_c=(11\pm.1)$ K at 1.2 T. Using $T_c=11$ K and the above fitting result, we obtain the value $2\Delta_0=(3.4\pm0.5)k_BT_c$ which is close to the BCS value, $2\Delta_0=3.52k_BT_c$. It is noted that the $(T_1T)^{-1}$ datum at 4 K is larger than the BCS prediction [see Fig. 14(b)]; this deviation may be due to the presence of a small temperature-independent contribution to the NSLR arising from paramagnetic impurities. Our value of $2\Delta_0/k_BT_c=3.4(5)$ is comparable with the values 3.9 (Refs. 13 and 14) and 4.2(1) (Ref. 15) determined calorimetrically for YNi_2B_2C, and 3.9 (Ref. 38) and 3.5 (Ref. 39) from electron tunneling measurements.

V. SUMMARY AND CONCLUSIONS

From the combination of ^{11}B, ^{89}Y NMR and magnetic susceptibility measurements, we have obtained detailed information on the electronic properties and structure of YNi_2B_2C in the normal metallic state. Both the small isotropic contact and anisotropic hyperfine constant at the B site are explained by the local electronic structure at the B site. The negative hyperfine interaction at the ^{89}Y site is consistent with a transferred hyperfine interaction involving polarization of *s*-like electrons at the Y site by *d* electrons.

We find a temperature-dependent and anisotropic spin susceptibility χ^{sp}. The temperature dependence of χ^{sp} is explained in terms of a narrow *d*-band structure with high density of *d* states at the Fermi level. The small anisotropy of χ^{sp} in this three-dimensional system is most likely due to asymmetry of the *g* factor. The temperature-independent Van Vleck contribution to the measured susceptibility is found to be large and strongly anisotropic. Both features are reproduced very well by theoretical calculations which in other respects are similar to previous calculations of the electronic band structure of the compound.

From the temperature dependence of the ^{11}B Knight shift we infer an unusually strong temperature dependence of the spin susceptibility due to boron *s* electrons, $\chi^{sp}_{B,s}(T)$. The band calculation predicts that $\chi^{sp}_{B,s}$ at the boron site has a much weaker *T* dependence than expected from the temperature dependence of the ^{11}B Knight shift. This remaining discrepancy may indicate that thermal expansion effects need to be included in the band theory calculations. It is also possible that the atomic-sphere-approximation linear-muffin-tin orbital method used here does not give a completely reliable result for the total energy of the system. Most importantly, we find that the enhancement in the ^{11}B NSLR simply reflects the increase of the spin susceptibility with lowering temperature and is not due to contributions of magnetic character from the Ni sublattice such as antiferromagnetic fluctuations of localized and/or itinerant electron spins. Thus we conclude that YNi_2B_2C is different from the cuprate high-T_C superconductors in this respect.

In the superconducting state, the ^{11}B NSLR is found to fit a BCS temperature dependence with a superconducting gap parameter at $T=0$ K, $2\Delta_0=(3.4\pm0.5)k_BT_c$, as expected from the normal properties of the Fermi liquid in the normal state. Although YNi_2B_2C behaves as a conventional type-II superconductor, no Hebel-Slichter coherence peak could be detected at the lowest magnetic field (0.9 T) at which the ^{11}B NSLR measurements could be performed.

ACKNOWLEDGMENTS

We thank K.-H. Kim and Q. Hu for their efforts in the beginning stage of the measurements. Ames Laboratory is operated for the U.S. Department of Energy by Iowa State University under Contract No. W-7405-Eng-82. This work was supported by the Director for Energy Research, Office of Basic Energy Sciences.

*Present address: MS K764, Los Alamos National Laboratory, Los Alamos, NM 87545.
†Also at Dipartimento di Fisica, Università di Pavia, 27100 Pavia, Italy.
‡Deceased.
§Present address: Department of Chemistry, Cornell University, Ithaca, NY 14853.
**Present address: Department of Physics, College of Natural Science, Hoseo University, Asan, 336-795 Choongnam, Korea.

[1] R. Nagarajan, C. Mazumdar, Z. Hossain, S. K. Dhar, K. V. Gopalakrishnan, L. C. Gupta, C. Godart, B. D. Padalia, and R. Vijayaraghavan, Phys. Rev. Lett. **72**, 274 (1994).
[2] R. J. Cava, H. Takagi, H. W. Zandbergen, J. J. Krajewski, W. F. Peck, Jr., T. Siegrist, B. Batlogg, R. B. van Dover, R. J. Felder, K. Mizuhashi, J. O. Lee, H. Eisaki, and S. Uchida, Nature **367**, 252 (1994).
[3] H. C. Ku, C. C. Lai, Y. B. You, J. H. Shieh, and W. Y. Guan, Phys. Rev. B **50**, 351 (1994); C. C. Lai, M. S. Lin, Y. B. You, and H. C. Ku, *ibid*. **51**, 420 (1995).
[4] J. L. Sarrao, M. C. de Andrade, J. Herrmann, S. H. Han, Z. Fisk, M. B. Maple, and R. J. Cava, Physica C **229**, 65 (1994).
[5] B. K. Cho, P. C. Canfield, and D. C. Johnston, Phys. Rev. B **52**, 3844R (1995); M. S. Lin, J. H. Shieh, Y. B. You, Y. Y. Hsu, J. W. Chen, S. H. Lin, Y. D. Yao, Y. Y. Chen, J. C. Ho, and H. C. Ku, Physica C **249**, 403 (1995); C. V. Tomy, G. Balakrishnan, and D. McK. Paul, *ibid*. **248**, 349 (1995).
[6] T. Siegrist, H. W. Zandbergen, R. J. Cava, J. J. Krajewski, and W. F. Peck, Jr., Nature **367**, 254 (1994).
[7] L. F. Mattheiss, Phys. Rev. B **49**, 13 279 (1994).
[8] W. E. Pickett and D. J. Singh, Phys. Rev. Lett. **72**, 3702 (1994); **74**, 3303(E) (1995).
[9] J. I. Lee, T. S. Zhao, I. G. Kim, B. I. Min, and S. J. Youn, Phys. Rev. B **50**, 4030 (1994).
[10] R. Coehoorn, Physica C **228**, 331 (1994).
[11] H. Kim, C.-D. Hwang, and J. Ihm, Phys. Rev. B **52**, 4592 (1995).
[12] P. Ravindran, S. Sankaralingam, and C. Asokamani, Phys. Rev. B **52**, 12 921 (1995).
[13] R. Movshovich, M. F. Hundley, J. D. Thompson, P. C. Canfield, B. K. Cho, and A. V. Chubukov, Physica C **227**, 381 (1994).
[14] N. M. Hong, H. Michor, M. Vybornov, T. Holubar, P. Hundegger, W. Perthold, G. Hilscher, and P. Rogl, Physica C **227**, 85 (1994); G. Hilscher, T. Holubar, N. M. Hong, W. Perthold, M. Vybornov, and P. Rogl, J. Magn. Magn. Mater. **140-144**, 2055 (1995).
[15] H. Michor, T. Holubar, C. Dusek, and G. Hilscher, Phys. Rev. B **52**, 16 165 (1995).
[16] S. A. Carter, B. Batlogg, R. J. Cava, J. J. Krajewski, W. F. Peck, Jr., and H. Takagi, Phys. Rev. B **50**, 4216 (1994).
[17] F. Borsa, Q. Hu, K. H. Kim, B. J. Suh, D. R. Torgeson, P. Canfield, M. Xu, and B. Zhong, Physica C **235-240**, 2547 (1994).
[18] M. E. Hanson, F. Lefloch, W. H. Wong, W. G. Clark, M. D. Lan, C. C. Hoellwarth, P. Klavins, and R. N. Shelton, Phys. Rev. B **51**, 674 (1995).
[19] K. Ikushima, J. Kikuchi, H. Yasuoka, R. J. Cava, H. Takagi, J. J. Krajewski, and W. W. Peck, Jr., J. Phys. Soc. Jpn. **63**, 2878 (1994).
[20] T. Kohara, T. Oda, K. Ueda, Y. Yamada, A. Mahajan, K. Elankumaran, Z. Hossian, L. C. Gupta, R. Nagarajan, R. Vijayaraghavan, and C. Mazumdar, Phys. Rev. B **51**, 3985 (1995).
[21] B. J. Suh, F. Borsa, D. R. Torgeson, B. K. Cho, P. C. Canfield, D. C. Johnston, J. Y. Rhee, and B. N. Harmon, Phys. Rev. B **53**, 6022R (1996).
[22] B. K. Cho, P. C. Canfield, L. L. Miller, D. C. Johnston, W. P. Beyermann, and A. Yatskar, Phys. Rev. B **52**, 3684 (1995); B. K. Cho, Ph.D. thesis, Iowa State University, 1995.
[23] G. C. Carter, L. H. Bennett, and D. J. Kahan, *Metallic Shifts in NMR* (Pergamon, New York, 1977), Pt. I.
[24] S. Chikazumi, *Physics of Magnetism* (Krieger, Huntington, 1978).
[25] A. Abragam, *Principles of Nuclear Magnetism* (Oxford, New York, 1961).
[26] P. W. Selwood, *Magnetochemistry*, 2nd ed. (Interscience, New York, 1956), p. 78.
[27] J. Benkowitsch and H. Winter, J. Phys. F **13**, 991 (1983).
[28] J. Y. Rhee, X. Wang, and B. N. Harmon, Phys. Rev. B **51**, 15 585 (1995).
[29] N. W. Ashcroft and N. D. Mermin, *Solid State Physics* (Holt, Rinehart, and Winston, New York, 1976), p. 669.
[30] D. C. Johnston and B. G. Silbernagel, Phys. Rev. B **21**, 4996 (1980).
[31] N. Bloembergen and T. J. Rowland, Acta Metall. **1**, 731 (1953); **3**, 74(E) (1955).
[32] H. Alloul, T. Ohno, and P. Mendels, Phys. Rev. Lett. **63**, 1700 (1989).
[33] T. T. Phua, B. J. Beaudry, D. T. Peterson, D. R. Torgeson, R. G. Barnes, M. Belhoul, G. A. Styles, and E. F. W. Seymour, Phys. Rev. B **28**, 627 (1983).
[34] R. W. Shaw and W. W. Warren, Phys. Rev. B **3**, 1562 (1971).
[35] T. Moriya, Prog. Theor. Phys. **16**, 23 (1956); **28**, 371 (1962).
[36] L. C. Hebel and C. P. Slichter, Phys. Rev. **113**, 1504 (1959).
[37] D. E. MacLaughlin, in *Solid State Physics*, edited by H. Ehrenreich, F. Seitz, and D. Turnbull (Academic, New York, 1976), Vol. **31**, p. 34.
[38] G. T. Jeong, J. I. Kye, S. H. Chun, Z. G. Khim, W. C. Lee, P. C. Canfield, B. K. Cho, and D. C. Johnston, Physica C **253**, 48 (1995).
[39] T. Fkino, H. Eujii, M. Kosugi, Y. Zenitani, and J. Akimitsu, Phys. Rev. B **53**, 5640 (1996); Physica C **235-240**, 2529 (1994).